

Light-Front Field Theory on Current Quantum Computers

Michael Kreshchuk ¹, Shaoyang Jia ^{2,3}, William M. Kirby ¹, Gary Goldstein ¹, James P. Vary ²
and Peter J. Love ^{1,4,*}

- ¹ Department of Physics and Astronomy, Tufts University, Medford, MA 02155, USA; michael.kreshchuk@tufts.edu (M.K.); William.Kirby@tufts.edu (W.M.K.); Gary.Goldstein@tufts.edu (G.G.)
² Department of Physics and Astronomy, Iowa State University, Ames, IA 50011, USA; syjia@anl.gov (S.J.); jvary@iastate.edu (J.P.V.)
³ Physics Division, Argonne National Laboratory, Argonne, IL 60439, USA
⁴ Computational Science Initiative, Brookhaven National Laboratory, Upton, NY 11973, USA
* Correspondence: peter.love@tufts.edu

Abstract: We present a quantum algorithm for simulation of quantum field theory in the light-front formulation and demonstrate how existing quantum devices can be used to study the structure of bound states in relativistic nuclear physics. Specifically, we apply the Variational Quantum Eigensolver algorithm to find the ground state of the light-front Hamiltonian obtained within the Basis Light-Front Quantization (BLFQ) framework. The BLFQ formulation of quantum field theory allows one to readily import techniques developed for digital quantum simulation of quantum chemistry. This provides a method that can be scaled up to simulation of full, relativistic quantum field theories in the quantum advantage regime. As an illustration, we calculate the mass, mass radius, decay constant, electromagnetic form factor, and charge radius of the pion on the IBM Vigo chip. This is the first time that the light-front approach to quantum field theory has been used to enable simulation of a real physical system on a quantum computer.



Citation: Kreshchuk, M.; Jia, S.; Kirby, W.M.; Goldstein, G.; Vary, J.P.; Love, P.J. Light-Front Field Theory on Current Quantum Computers. *Entropy* **2021**, *23*, 597. <https://doi.org/10.3390/e23050597>

Academic Editor: Leong Chuan Kwek

Received: 7 April 2021
Accepted: 5 May 2021
Published: 12 May 2021

Publisher's Note: MDPI stays neutral with regard to jurisdictional claims in published maps and institutional affiliations.



Copyright: © 2021 by the authors. Licensee MDPI, Basel, Switzerland. This article is an open access article distributed under the terms and conditions of the Creative Commons Attribution (CC BY) license (<https://creativecommons.org/licenses/by/4.0/>).

Keywords: quantum simulation; relativistic bound states; hadrons; mesons; BLFQ; light-front; VQE

1. Introduction

The light-front quantization framework of quantum field theories (QFTs) is well-adapted for digital quantum simulation. We demonstrated this in our previous work by developing quantum algorithms based on simulating time evolution and adiabatic state preparation [1]. In the present paper, we aim for near-term devices by showing how to formulate the relativistic bound state problem as an instance of the Variational Quantum Eigensolver (VQE) algorithm [2–21]. VQE is a hybrid quantum-classical algorithm for finding low-lying eigenvalues and eigenstates of a given Hamiltonian, which can be implemented on existing quantum computers. We are thus able to run example simulations on IBM Vigo, one of IBM's publicly available quantum processors. Similar to [20], we apply VQE to a two-body bound state in nuclear physics using Hamiltonian dynamics [22]. However, we consider here deeply bound states of quarks in mesons with relativistic kinematics, instead of the weakly bound deuteron studied in [20].

For an efficient Hamiltonian formulation of quantum field theory, we use the framework of Basis Light-Front Quantization (BLFQ) [23,24] and choose a basis tailored to the symmetries and dynamics specific to a particular physical system. Having much in common with *ab initio* methods in quantum chemistry and nuclear theory, it serves as an ideal framework for testing near-term devices by solving problems such as calculation of hadronic spectra [25–28] and parton distribution functions [29–31].

Within BLFQ, a field is expanded in terms of second-quantized Fock states representing occupancies of modes (first-quantized basis functions), and there is no *a priori* limit on the degrees of freedom [23]. Accordingly, our algorithms are designed to efficiently simulate QFT applications where particle number is not conserved. However, for QFTs at

low resolution or for phenomenological applications, BLFQ is often restricted to the valence degrees of freedom, so we adopt this restriction in order to implement quantum simulations on an existing quantum chip. These experiments represent the first stage shown in Figure 1, which illustrates a progression of methods that scale towards fault-tolerant simulation of QFTs in the quantum supremacy regime. However, the methods we propose apply to the first three stages in Figure 1, while the final stage was discussed in [1]. In other words, in this paper we describe techniques that may be used to simulate bound states of general quantum field theories in the full multi-particle setting.

For our experimental demonstration, we consider the dynamics of valence quarks for light mesons on the light front using the Hamiltonian from [32]. This Hamiltonian includes the kinetic energy, the confinement potential in both the longitudinal and the transverse directions [28], and the Nambu–Jona-Lasinio (NJL) interaction [33] to account for the chiral interactions among quarks. The dependence of the light-front wave functions for valence quarks on the relative momentum is expanded in terms of the adopted modes, which are orthonormal basis functions. After imposing finite cut-offs in this expansion, the light-front Hamiltonian becomes a Hermitian matrix in the resulting basis representation. We use the same scheme as in [32] to fix our model parameters at each choice of basis cut-offs.

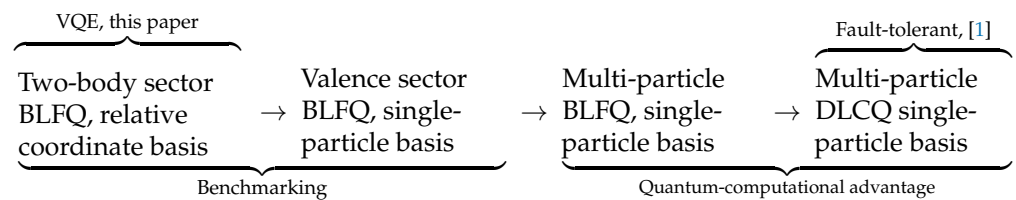


Figure 1. Quantum simulation of the light-front quantum field theory at different stages of complexity and resource requirements. Discrete light-cone quantization (DLCQ) [34] may be considered to be a special case of BLFQ [23] that employs a plane-wave basis, and may be useful in the fault-tolerant quantum computing regime [1]. We separate the rightmost (DLCQ) stage because classical preprocessing is used in BLFQ to obtain approximations using fewer quantum resources.

We implement VQE for this model on the IBM Vigo processor. We minimize the mass-squared of a pion obtained from a variational ansatz for its wave function. Using the resulting ansatz, we compute the decay constant, mass radius, and elastic form factor of the pion on the quantum processor. We thus demonstrate that the light-front formulation of QFT enables calculations of properties of composite particles in relativistic field theories on existing quantum processors.

2. Basis Light-Front Quantization

In the Hamiltonian framework of light-front quantum field theories, the bound state spectrum is obtained as the eigenvalues of the mass squared operator $M^2 = P^i P_i$:

$$P^j P_j |\Psi\rangle = (P^+ P^- - \mathbf{P}_\perp^2) |\Psi\rangle = m^2 |\Psi\rangle, \tag{1}$$

where $P^+ = P^0 + P^3$ and \mathbf{P}_\perp are the conserved light-front longitudinal momentum and transverse momenta, respectively. On the other hand, $P^- = P^0 - P^3$ is the light-front Hamiltonian, which, when included in M^2 , forms an effective Hamiltonian whose eigenvalues are m^2 . The eigenvectors of (1) are known as the light-front wave functions (LFWFs), from which one can determine various observables.

In the present work, we apply the light-front formalism to studying hadrons. While one can, in principle, use the fundamental quantum chromodynamics (QCD) Hamiltonian, in the current paper we solve for the relative momentum LFWFs of the valence quarks inside light mesons, using the effective Hamiltonian from [32]. In this Hamiltonian, the

confinement of quarks inside the hadrons is based on the anti-de Sitter Space/quantum chromodynamics (AdS/QCD) correspondence [35,36].

To construct the effective Hamiltonian operator, we start from the *soft-wall* AdS/QCD Hamiltonian, describing the dynamics of valence quarks [35,36], which assumes zero quark masses and a transverse confining potential:

$$H_{\text{SW}} = P^+ P_{\text{SW}}^- - \mathbf{P}_\perp^2 = \frac{\vec{\kappa}_\perp^2}{x(1-x)} + b^4 x(1-x) \vec{r}_\perp^2, \quad (2)$$

where the operator $x = k^+ / P^+$ corresponds to the longitudinal momentum fraction carried by the valence quark, b specifies the strength of the confinement potential, $\vec{\kappa}_\perp^2 = \vec{k}_\perp^2 - x \vec{P}_\perp^2$ is the operator of relative transverse momentum of the valence quarks, and the operator \vec{r}_\perp^2 is conjugate to $\vec{\kappa}_\perp^2$. k^μ are the components of the valence quark four-momentum operator.

While the Hamiltonian (2) is only designed to act on the meson valence sector wave function (7) to be introduced below, by using the single-particle basis [23], BLFQ allows one to extend the AdS/QCD LFWFs and effective interactions to the multi-particle Fock sectors [23,37–39]. This is crucial for quantum-computing applications, since we only expect to attain quantum advantage in the multi-particle regime.

Next, we modify H_{SW} in (2) by adding nonzero quark masses and effective longitudinal confinement [25,28]:

$$H_{\text{SW}} \rightarrow H_0 = H_{\text{SW}} + \frac{\mathbf{m}}{x} + \frac{\bar{\mathbf{m}}}{1-x} - \frac{b^4}{(\mathbf{m} + \bar{\mathbf{m}})^2} \partial_x x(1-x) \partial_x, \quad (3)$$

where \mathbf{m} and $\bar{\mathbf{m}}$ are the masses of the valence quark and valence antiquark, respectively. The form of longitudinal potential is chosen so that it would reduce to the three-dimensional harmonic oscillator potential in the non-relativistic limit. Allowing an independent coupling parameter for the longitudinal confinement in (3) can be fruitful for describing multiple meson sectors [40].

The remaining part of the strong interaction between quarks, $H_{\text{int}}^{\text{eff}}$, is modeled using the scalar-pseudoscalar channel of the color-singlet NJL model [33]. Thus, we end up with a Hamiltonian of the form

$$H^{\text{eff}} = H_0 + H_{\text{int}}^{\text{eff}}, \quad (4)$$

where H^{eff} takes the role of $P^j P_j$ in Equation (1) in the valence Fock sector of mesons (two-quark bound states) with

$$H_0 = \frac{(\vec{\kappa}_\perp^2)^2 + \mathbf{m}^2}{x} + \frac{(\vec{\kappa}_\perp^2)^2 + \bar{\mathbf{m}}^2}{1-x} + b^4 x(1-x) \vec{r}_\perp^2 - \frac{b^4}{(\mathbf{m} + \bar{\mathbf{m}})^2} \partial_x x(1-x) \partial_x \quad (5)$$

containing kinematic terms and two-body confining potentials. For clarity we introduce the interaction in terms of field operators as

$$H_{\text{int}}^{\text{eff}} = \int dx^- \int d\vec{x}_\perp \left(-\frac{G_\pi P^+}{2} \right) \left[(\bar{\psi}\psi)^2 + (\bar{\psi}i\gamma_5 \vec{\tau} \psi)^2 \right], \quad (6)$$

which absorbs quark-gluon and gluon-gluon QCD couplings into local four-fermion self-interactions. When applied to Equation (4), an expansion into the valence Fock sector of mesons is implied for Equation (6). In (6) x^- and \vec{x}_\perp are the single-particle light-front coordinates, $\vec{\tau}$ consists of the Pauli spin operators acting in the isospin space on the fermion field operator ψ , G_π is the NJL coupling constant, and the normal ordering of H^{eff} is understood.

Within the BLFQ, the LFWFs of the valence quarks are expressed as [32]

$$\begin{aligned} |\Psi(P^+, \vec{P}^\perp)\rangle &= \sum_{r,s} \int_0^1 \frac{dx}{4\pi x(1-x)} \\ &\times \int \frac{d\vec{\kappa}^\perp}{(2\pi)^2} \psi_{rs}(x, \vec{\kappa}^\perp) \times b_r^\dagger(xP^+, \vec{\kappa}^\perp + x\vec{P}^\perp) \\ &\times d_s^\dagger((1-x)P^+, -\vec{\kappa}^\perp + (1-x)\vec{P}^\perp) |0\rangle. \end{aligned} \quad (7)$$

The ladder operators b_r^\dagger and d_r^\dagger create a quark and an antiquark of spin r from the light-front vacuum, and obey the usual anticommutation relations $\{b_r, b_s^\dagger\} = \{d_r, d_s^\dagger\} = \delta_{rs}$ (all other anticommutators being zero). The light-front wave function for the valence quarks is then expanded in the following orthonormal basis:

$$\psi_{rs}(x, \vec{\kappa}^\perp) = \sum_{nml} \psi(n, m, l, r, s) \phi_{nm} \left(\frac{\vec{\kappa}^\perp}{\sqrt{x(1-x)}}; b \right) \chi_l(x), \quad (8)$$

where ϕ_{nm} is a two-dimensional (2D) harmonic oscillator eigenfunction, χ_l is the longitudinal basis function related to Jacobi polynomials [32], and n , m , and l are the radial, angular, and longitudinal basis quantum numbers respectively. The momentum scale of the harmonic oscillator function is chosen identical to the confinement strength in Equation (5). In the representation in which analytic expressions exist for these basis functions, H_0 is diagonal. Furthermore, the matrix elements of the full Hamiltonian (4) in this representation can be calculated analytically [32].

3. Mapping onto Qubits

To simulate the BLFQ Hamiltonian described above, we will use the variational quantum eigensolver (VQE) algorithm, which can be implemented on existing quantum computers. VQE is an approach to finding Hamiltonian eigenvalues, in which a quantum processor is used as part of a hybrid quantum-classical algorithm [4]. In VQE, a quantum computer is used to evaluate the Hamiltonian expectation value for a given variational state, while a classical computer performs a gradient search to minimize the expectation value. In order to formulate a physical problem as a VQE instance, one has to (a) Establish a correspondence between the physical states and the multi-qubit states of a quantum computer, (b) Prepare a parametrized ansatz state on the quantum computer $|\psi(\vec{\theta})\rangle = U(\vec{\theta})|\psi_0\rangle$ ($|\psi_0\rangle$ is some easy to prepare reference state), (c) Evaluate the Hamiltonian expectation value $E(\vec{\theta}) = \langle \psi(\vec{\theta}) | \hat{H} | \psi(\vec{\theta}) \rangle$ by sampling on the quantum computer, (d) Send the estimated value $E(\vec{\theta})$ to the classical optimization to determine the set of parameters for the next iteration of the algorithm. VQE has been successfully applied to finding the ground states of second-quantized Hamiltonians in quantum chemistry [4,7,21,41].

In order to apply VQE, we first need to map our Hamiltonian of interest to a qubit Hamiltonian. Written as an operator acting on valence sector Fock states, the Hamiltonian (4) is a fourth-order polynomial in quark and antiquark creation and annihilation operators. Thus it resembles the general form of Hamiltonians in quantum chemistry, $H = \sum_{i,j} h_{ij} a_i^\dagger a_j + \sum_{i,j,k,l} h_{ijkl} a_i^\dagger a_j^\dagger a_k a_l$, where a^\dagger is a fermionic operator, which in our case could create either a quark or antiquark. This remains true as one extends the problem to multi-particle Fock states, and enables us to use methods developed for digital quantum simulation of quantum chemistry [4]. However, the restriction to the valence sector Fock states (7) is special in the sense that in this reduced subspace the Hamiltonian can be written in terms of effective single-body interactions $H^{\text{eff}} = \sum_{i,j} h_{ij} c_i^\dagger c_j$, where the operators c_i^\dagger create two-body modes from vacuum. The c_i^\dagger and c_j are bosonic (meaning that they commute with each other), yet square to zero (owing to the fermionic nature of their constituents). However, we may treat them as fermionic operators because the distinction between commutation relations for fermionic and bosonic operators depends on the occupations of modes other than those they act upon, and the total occupancy in our case is limited to one.

Because we are aiming for multiparticle simulation of fermions, we therefore use fermionic mappings in order to provide a demonstration of techniques that we would use in the multi-particle scenario.

For the demonstrations below, we use the light meson BLFQ Hamiltonian with the minimal choice of basis function cutoffs and model parameters specified in Table 1. In the zero azimuthal angular momentum block, the Hamiltonian describes the interaction of quarks whose momentum-space wave function is in the lowest eigenstate of H_0 :

$$h_{ij} = \begin{pmatrix} 640,323 & 139,872 & -139,872 & -107,450 \\ 139,872 & 346,707 & 174,794 & 139,872 \\ -139,872 & 174,794 & 346,707 & -139,872 \\ -107,450 & 139,872 & -139,872 & 640,323 \end{pmatrix}, \quad (9)$$

where the matrix elements are in units of MeV^2 . The size of H reflects the 4 possible spin configurations of the valence quarks. In this case the NJL interaction takes the role of the spin-orbit interaction of quarks. The lowest eigenvalue of H corresponds to the squared mass of the pion, $m_\pi^2 = (139.6 \text{ MeV})^2$. Note that in the light-front formulation, the Hamiltonian is the invariant mass-squared operator [34].

Table 1. Model parameters of the BLFQ-NJL model. The antiquark mass is identical to the quark mass.

m	κ	G_π
337.01 MeV	227.00 MeV	250.785 GeV^{-2}

The expectation value of the Hamiltonian is calculated via its decomposition into Pauli operators P_i with real coefficients h_i :

$$\langle \psi(\vec{\theta}) | \hat{H} | \psi(\vec{\theta}) \rangle = \sum_i h_i \langle \psi(\vec{\theta}) | P_i | \psi(\vec{\theta}) \rangle. \quad (10)$$

The expectation values of the individual Pauli terms on the RHS of (10) can be efficiently measured via sampling from the state $|\psi(\vec{\theta})\rangle$ [4]. Various techniques for reducing the number of required measurements have been proposed [42–48], but for the purpose of our demonstration we simply estimate each Pauli expectation value separately.

We explore two approaches to simulation in the BLFQ formulation. The first uses *direct encoding* of Fock states in qubit states, meaning that the occupation of each mode is represented in a fixed register of qubits. Since we are using the relative momentum basis and working within the valence sector of the Fock space, the basis Fock states only contain one occupied mode. We employ the Jordan-Wigner (JW) encoding [49], which is commonly used in quantum chemistry [50,51], and in our case simply means encoding the occupation of each mode in a single qubit. Any superposition of such encoded states can be prepared using the simple circuit given in Figure 2a. For multi-particle states, one could switch to the more efficient Bravyi-Kitaev encoding [52,53], and use the Unitary Coupled Cluster ansatz [41]. In direct encodings, the number of qubits required for the simulation is equal to the number of fermionic modes in the Fock state, which scales as the product of the cutoffs for the (n, m, l) quantum numbers [32].

A different approach is based on *compact encoding* [1,50], in which only the quantum numbers of occupied modes are stored; in our case, this amounts to storing the index of the single occupied mode in binary form. Therefore, the number of qubits required for storing a single-particle Fock state is logarithmic in the number of modes, and so the number of parameters required for arbitrary state preparation is polynomial in the number of modes. Thus, one can express Hamiltonian (9) in terms of two-qubit Pauli operators, and use arbitrary state preparation as an ansatz circuit, as shown in Figure 2b.

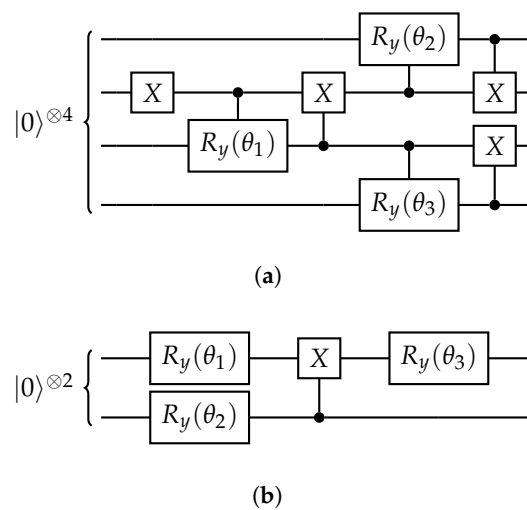


Figure 2. Ansatz circuits for preparing an arbitrary superposition of single-particle Fock states with real coefficients in the direct encoding (a) and compact encoding (b). $R_y(\theta)$ denotes a single-qubit rotation through an angle θ about the y -axis.

In the multi-particle case, in compact encoding, the number of Pauli terms in the qubit Hamiltonian may become exponential in the system size. However, the Hamiltonian matrix in the basis of Fock states is sparse because it contains polynomially many creation and annihilation operator monomials, and each of these connects a Fock state to, at most, one other Fock state. Therefore, we can use the formulation of VQE for sparse Hamiltonians described in [54] for the multi-particle compact encoding case.

4. Results

We implemented VQE on the IBM Vigo quantum processor using both direct and compact encodings with and without measurement error mitigation provided by Qiskit [55]. In Figure 3, we show the experimentally obtained energies at each minimization step, as well as the exact values and those obtained by classical sampling from the exact probability distributions (the latter illustrates the performance of a noiseless quantum computer). The improvement due to measurement error mitigation was significant only for the compact encoding, and led to the best convergence to the true ground state energy out of the experimental methods.

We evaluated additional observables in the ground state. In Table 2, we show the accuracies obtained using each technique: exact evaluation, classical sampling, and sampling on the IBM Vigo chip with and without measurement error mitigation. We prepared the ground state on the IBM Vigo chip by using the parameters obtained in our VQE minimization. The observables we measured are the pion mass, mass radius, and decay constant. As expected, the results obtained using the compact encoding are consistently more accurate than those obtained using the direct encoding, since the corresponding ansatz circuits are shorter. Measurement error mitigation consistently improves the accuracies in the compact encoding, and provides no benefit in the direct encoding. However, we do see that in nearly all cases, the quantum methods are approximately correct, with the method using compact encoding and measurement error mitigation approaching the performance of classical sampling.

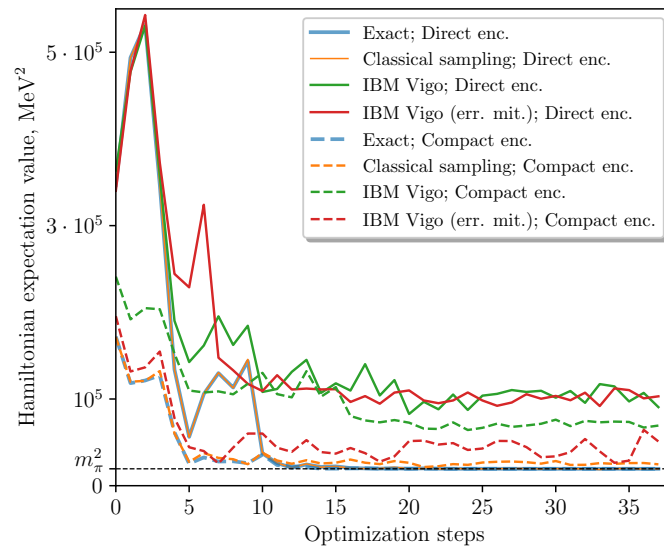


Figure 3. Results of the VQE minimization algorithm in the compact and direct encodings. Each point was obtained from 8192 samples per term on the IBM Vigo chip. Note that here $m_\pi^2 = (139.6 \text{ MeV})^2$ is the lowest eigenvalue of the Hamiltonian, by definition (see (9) and the associated discussion).

Table 2. Fractional errors, expressed as percentages, in estimates of various observables calculated in the ground state obtained by means of the VQE minimization. The observables are pion mass squared (m_π^2), mass radius squared ($\langle r_m \rangle^2$), and decay constant (f_π). These were obtained from 8192 samples per term on the IBM Vigo chip, with and without measurement error mitigation. Classical sampling means sampling from the exact probability distribution. Observables are shown both including constant terms (the physically relevant values), and not including them (the measured values). The constant terms are different between direct and compact encodings, therefore direct and compact entries in “no constant” rows correspond to different physical observables, and should not be compared. For m_π^2 , the exact m_ρ^2 is used for normalization, where m_ρ^2 , the mass of the rho meson squared, is the second lowest eigenvalue of the light meson BLFQ Hamiltonian.

	Direct Encoding			Compact Encoding		
	Classical Sampling	IBM Vigo	IBM Vigo, err. mit.	Classical Sampling	IBM Vigo	IBM Vigo, err. mit.
m_π^2 , no constant	0.48%	7.6%	7.5%	0.01%	11.6%	6.2%
m_π^2	0.90%	14.1%	14.0%	0.08%	12.7%	9.1%
$\langle r_m \rangle^2$, no constant	0.45%	6.6%	7.2%	0.43%	29.4%	7.1%
$\langle r_m \rangle^2$	0.65%	9.5%	10.4%	0.01%	6.4%	1.6%
f_π , no constant	0.05%	59.8%	59.0%	0.21%	29.2%	7.6%
f_π	0.02%	21.0%	20.7%	0.14%	13.0%	5.1%

We computed the pion elastic form factor $F(Q^2)$, obtaining the results shown in Figure 4. Based on these data, we computed the pion charge radius as $\langle r_c^2 \rangle = -6 dF(Q^2) / dQ^2|_{Q^2=0}$. The values obtained using the quantum computer match those obtained via the state vector representation, $\sqrt{\langle r_c^2 \rangle} = 1.24 \text{ fm}$, within a few percent precision. These calculations illustrate that our algorithm provides reasonable results for physically meaningful quantities even with the noisy and limited quantum resources that are currently available.

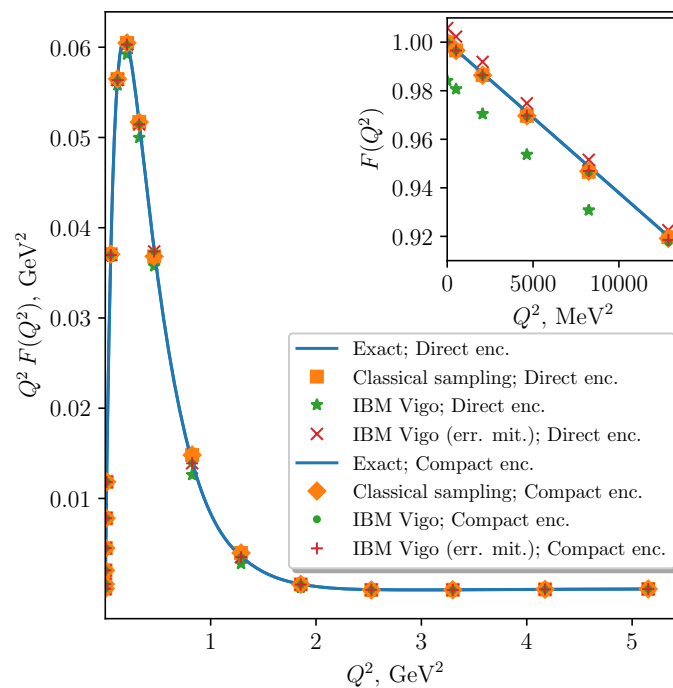


Figure 4. Pion elastic form factor, obtained from 8192 samples per term on the IBM Vigo processor, with and without measurement error mitigation.

5. Discussion

In this work, we demonstrated how one can use existing quantum processors to perform calculations in relativistic field theories in the light-front formulation. The methods we proposed apply to the multi-particle setting, which can potentially reach the regime of quantum advantage. While designing a scalable VQE ansatz for the compact encoding remains an open problem, using the direct encoding allows one to readily employ techniques developed for digital simulation of quantum chemistry. We have thus demonstrated the viability of quantum simulation in the light-front formulation, using methods that can be scaled to exploit the available quantum resources, from existing noisy intermediate-scale quantum machines up to the crossover into fault-tolerance.

Author Contributions: Each co-author contributed equally to the work. All authors have read and agreed to the published version of the manuscript.

Funding: W.M.K. acknowledges support from the National Science Foundation, Grant No. DGE-1842474. P.J.L. and M.K. and G.G. acknowledge support from DOE HEP Grant No. DE-SC0019452. S.J. and J.P.V. acknowledge support from DOE Grant Nos. DE-FG02-87ER40371 and DE-SC0018223. S.J. also acknowledges support from DOE Office of Science, Office of Nuclear Physics, contract No. DE-AC02-06CH11357. This work was supported by the NSF STAQ project (PHY-1818914).

Data Availability Statement: The data and scripts that support the findings of this study are available from the corresponding author upon reasonable request. Circuit diagrams are rendered using the LATEX Quantikz package [56], and 2D plots are generated with the Python matplotlib package [57].

Conflicts of Interest: The authors declare no conflict of interest.

References

1. Kreshchuk, M.; Kirby, W.M.; Goldstein, G.; Beauchemin, H.; Love, P.J. Quantum Simulation of Quantum Field Theory in the Light-Front Formulation. *arXiv* **2020**, arXiv:2002.04016.
2. Du, J.; Xu, N.; Peng, X.; Wang, P.; Wu, S.; Lu, D. NMR Implementation of a Molecular Hydrogen Quantum Simulation with Adiabatic State Preparation. *Phys. Rev. Lett.* **2010**, *104*, 030502, doi:10.1103/PhysRevLett.104.030502.
3. Lanyon, B.P.; Whitfield, J.D.; Gillett, G.G.; Goggin, M.E.; Almeida, M.P.; Kassal, I.; Biamonte, J.D.; Mohseni, M.; Powell, B.J.; Barbieri, M.; et al. Towards quantum chemistry on a quantum computer. *Nat. Chem.* **2010**, *2*, 106–111.
4. Peruzzo, A.; McClean, J.; Shadbolt, P.; Yung, M.H.; Zhou, X.Q.; Love, P.J.; Aspuru-Guzik, A.; O'Brien, J.L. A variational eigenvalue solver on a photonic quantum processor. *Nat. Commun.* **2014**, *5*, 4213.
5. Wang, Y.; Dolde, F.; Biamonte, J.; Babbush, R.; Bergholm, V.; Yang, S.; Jakobi, I.; Neumann, P.; Aspuru-Guzik, A.; Whitfield, J.D.; et al. Quantum simulation of helium hydride cation in a solid-state spin register. *ACS Nano* **2015**, *9*, 7769–7774.
6. O'Malley, P.J.J.; Babbush, R.; Kivlichan, I.D.; Romero, J.; McClean, J.R.; Barends, R.; Kelly, J.; Roushan, P.; Tranter, A.; Ding, N.; et al. Scalable Quantum Simulation of Molecular Energies. *Phys. Rev. X* **2016**, *6*, 031007, doi:10.1103/PhysRevX.6.031007.
7. McClean, J.R.; Romero, J.; Babbush, R.; Aspuru-Guzik, A. The theory of variational hybrid quantum-classical algorithms. *New J. Phys.* **2016**, *18*, 023023.
8. Santagati, R.; Wang, J.; Gentile, A.A.; Paesani, S.; Wiebe, N.; McClean, J.R.; Morley-Short, S.; Shadbolt, P.J.; Bonneau, D.; Silverstone, J.W.; et al. Witnessing eigenstates for quantum simulation of Hamiltonian spectra. *Sci. Adv.* **2018**, *4*, eaap9646. doi:10.1126/sciadv.aap9646.
9. Shen, Y.; Zhang, X.; Zhang, S.; Zhang, J.N.; Yung, M.H.; Kim, K. Quantum implementation of the unitary coupled cluster for simulating molecular electronic structure. *Phys. Rev. A* **2017**, *95*, 020501.
10. Paesani, S.; Gentile, A.A.; Santagati, R.; Wang, J.; Wiebe, N.; Tew, D.P.; O'Brien, J.L.; Thompson, M.G. Experimental Bayesian Quantum Phase Estimation on a Silicon Photonic Chip. *Phys. Rev. Lett.* **2017**, *118*, 100503, doi:10.1103/PhysRevLett.118.100503.
11. Hempel, C.; Maier, C.; Romero, J.; McClean, J.; Monz, T.; Shen, H.; Jurcevic, P.; Lanyon, B.P.; Love, P.J.; Babbush, R.; et al. Quantum Chemistry Calculations on a Trapped-Ion Quantum Simulator. *Phys. Rev. X* **2018**, *8*, 031022, doi:10.1103/PhysRevX.8.031022.
12. Colless, J.I.; Ramasesh, V.V.; Dahlen, D.; Blok, M.S.; Kimchi-Schwartz, M.E.; McClean, J.R.; Carter, J.; de Jong, W.A.; Siddiqi, I. Computation of Molecular Spectra on a Quantum Processor with an Error-Resilient Algorithm. *Phys. Rev. X* **2018**, *8*, 011021, doi:10.1103/PhysRevX.8.011021.
13. Nam, Y.; Chen, J.S.; Pseni, N.C.; Wright, K.; Delaney, C.; Maslov, D.; Brown, K.R.; Allen, S.; Amini, J.M.; Apisdorf, J.; et al. Ground-state energy estimation of the water molecule on a trapped ion quantum computer. *NPJ Quantum Inf.* **2020**, *6*, 33.
14. Kokail, C.; Maier, C.; van Bijnen, R.; Brydges, T.; Joshi, M.K.; Jurcevic, P.; Muschik, C.A.; Silvi, P.; Blatt, R.; Roos, C.F.; et al. Self-verifying variational quantum simulation of lattice models. *Nature* **2019**, *569*, 355–360, doi:10.1038/s41586-019-1177-4.
15. Kandala, A.; Temme, K.; Córcoles, A.D.; Mezzacapo, A.; Chow, J.M.; Gambetta, J.M. Error mitigation extends the computational reach of a noisy quantum processor. *Nature* **2019**, *567*, 491–495, doi:10.1038/s41586-019-1040-7.
16. Google AI Quantum and Collaborators. Hartree-Fock on a superconducting qubit quantum computer. *Science* **2020**, *369*, 1084–1089, doi:10.1126/science.abb9811.
17. Nakanishi, K.M.; Mitarai, K.; Fujii, K. Subspace-search variational quantum eigensolver for excited states. *Phys. Rev. Res.* **2019**, *1*, 033062, doi:10.1103/PhysRevResearch.1.033062.
18. Tilly, J.; Jones, G.; Chen, H.; Wossnig, L.; Grant, E. Computation of molecular excited states on IBMQ using a Discriminative Variational Quantum Eigensolver. *Phys. Rev. A* **2020**, *102*, 062425.
19. Higgott, O.; Wang, D.; Brierley, S. Variational Quantum Computation of Excited States. *Quantum* **2019**, *3*, 156, doi:10.22331/q-2019-07-01-156.
20. Dumitrescu, E.F.; McCaskey, A.J.; Hagen, G.; Jansen, G.R.; Morris, T.D.; Papenbrock, T.; Pooser, R.C.; Dean, D.J.; Lougovski, P. Cloud Quantum Computing of an Atomic Nucleus. *Phys. Rev. Lett.* **2018**, *120*, 210501, doi:10.1103/PhysRevLett.120.210501.
21. Kandala, A.; Mezzacapo, A.; Temme, K.; Takita, M.; Brink, M.; Chow, J.M.; Gambetta, J.M. Hardware-efficient variational quantum eigensolver for small molecules and quantum magnets. *Nature* **2017**, *549*, 242–246.
22. Kreshchuk, M.; Jia, S.; Kirby W.M.; Goldstein G.; Vary J.P.; Love P.J. Simulating Hadronic Physics on NISQ devices using Basis Light-Front Quantization (accepted to *Phys. Rev. A*). *arXiv* **2020**, arXiv:2011.13443.
23. Vary, J.P.; Honkanen, H.; Li, J.; Maris, P.; Brodsky, S.J.; Harindranath, A.; de Teramond, G.F.; Sternberg, P.; Ng, E.G.; Yang, C. Hamiltonian light-front field theory in a basis function approach. *Phys. Rev. C* **2010**, *81*, 035205, doi:10.1103/PhysRevC.81.035205.
24. Zhao, X. Advances in Basis Light-front Quantization. *Few Body Syst.* **2015**, *56*, 257–265.
25. Li, Y.; Maris, P.; Zhao, X.; Vary, J.P. Heavy quarkonium in a holographic basis. *Phys. Lett. B* **2016**, *758*, 118–124, doi:10.1016/j.physletb.2016.04.065.
26. Tang, S.; Li, Y.; Maris, P.; Vary, J.P. B_c mesons and their properties on the light front. *Phys. Rev. D* **2018**, *98*, 114038, doi:10.1103/PhysRevD.98.114038.
27. Tang, S.; Li, Y.; Maris, P.; Vary, J.P. Heavy-light mesons on the light front. *Eur. Phys. J. C* **2020**, *80*, 522, doi:10.1140/epjc/s10052-020-8081-9.
28. Li, Y.; Maris, P.; Vary, J.P. Quarkonium as a relativistic bound state on the light front. *Phys. Rev. D* **2017**, *96*, 016022, doi:10.1103/PhysRevD.96.016022.

29. Lan, J.; Mondal, C.; Jia, S.; Zhao, X.; Vary, J.P. Parton Distribution Functions from a Light Front Hamiltonian and QCD Evolution for Light Mesons. *Phys. Rev. Lett.* **2019**, *122*, 172001, doi:10.1103/PhysRevLett.122.172001.
30. Lan, J.; Mondal, C.; Li, M.; Li, Y.; Tang, S.; Zhao, X.; Vary, J.P. Parton Distribution Functions of Heavy Mesons on the Light Front. *Phys. Rev. D* **2020**, *102*, 014020, doi:10.1103/PhysRevD.102.014020.
31. Lan, J.; Mondal, C.; Jia, S.; Zhao, X.; Vary, J.P. Pion and kaon parton distribution functions from basis light front quantization and QCD evolution. *Phys. Rev. D* **2020**, *101*, 034024, doi:10.1103/PhysRevD.101.034024.
32. Jia, S.; Vary, J.P. Basis light front quantization for the charged light mesons with color singlet Nambu–Jona-Lasinio interactions. *Phys. Rev. C* **2019**, *99*, 035206, doi:10.1103/PhysRevC.99.035206.
33. Klevansky, S.P. The Nambu–Jona-Lasinio model of quantum chromodynamics. *Rev. Mod. Phys.* **1992**, *64*, 649–708, doi:10.1103/RevModPhys.64.649.
34. Brodsky, S.J.; Pauli, H.C.; Pinsky, S.S. Quantum chromodynamics and other field theories on the light cone. *Phys. Rep.* **1998**, *301*, 299–486, doi:10.1016/S0370-1573(97)00089-6.
35. de Téramond, G.F.; Brodsky, S.J. Light-Front Holography: A First Approximation to QCD. *Phys. Rev. Lett.* **2009**, *102*, 081601, doi:10.1103/PhysRevLett.102.081601.
36. Brodsky, S.J.; de Téramond, G.F.; Dosch, H.G.; Erlich, J. Light-Front Holographic QCD and Emerging Confinement. *Phys. Rept.* **2015**, *584*, 1–105, doi:10.1016/j.physrep.2015.05.001.
37. Fu, K.; Zhao, H.; Zhao, X.; Vary, J.P. Positronium on the light front. In Proceedings of the 18th International Conference on Hadron Spectroscopy and Structure, Guilin, China, 16–21 August 2019. doi:10.1142/9789811219313_0093.
38. Zhao, X.; Fu, K.; Zhao, H.; Vary, J.P. Positronium: An illustration of nonperturbative renormalization in a basis light-front approach. *arXiv* **2020**, arXiv:2103.06719, doi:10.22323/1.374.0090.
39. Hu, Z.; Xu, S.; Mondal, C.; Zhao, X.; Vary, J.P. Transverse structure of electron in momentum space in basis light-front quantization. *Phys. Rev. D* **2021**, *103*, 036005, doi:10.1103/PhysRevD.103.036005.
40. Li, Y.; Vary, J.P. Light-front holography with chiral symmetry breaking. *arXiv* **2021**, arXiv:2103.09993.
41. Romero, J.; Babbush, R.; McClean, J.R.; Hempel, C.; Love, P.J.; Aspuru-Guzik, A. Strategies for quantum computing molecular energies using the unitary coupled cluster ansatz. *Quantum Sci. Technol.* **2018**, *4*, 014008, doi:10.1088/2058-9565/aad3e4.
42. Yen, T.C.; Verteletskyi, V.; Izmaylov, A.F. Measuring All Compatible Operators in One Series of Single-Qubit Measurements Using Unitary Transformations. *J. Chem. Theory Comput.* **2020**, *16*, 2400–2409, doi:10.1021/acs.jctc.0c00008.
43. Gokhale, P.; Angiuli, O.; Ding, Y.; Gui, K.; Tomesh, T.; Suchara, M.; Martonosi, M.; Chong, F.T. Minimizing State Preparations in Variational Quantum Eigensolver by Partitioning into Commuting Families. *arXiv* **2019**, arXiv:1907.13623.
44. Izmaylov, A.F.; Yen, T.C.; Lang, R.A.; Verteletskyi, V. Unitary Partitioning Approach to the Measurement Problem in the Variational Quantum Eigensolver Method. *J. Chem. Theory Comput.* **2019**, doi:10.1021/acs.jctc.9b00791.
45. Zhao, A.; Tranter, A.; Kirby, W.M.; Ung, S.F.; Miyake, A.; Love, P.J. Measurement reduction in variational quantum algorithms. *Phys. Rev. A* **2020**, *101*, 062322, doi:10.1103/PhysRevA.101.062322.
46. Bonet-Monroig, X.; Babbush, R.; O’Brien, T.E. Nearly Optimal Measurement Scheduling for Partial Tomography of Quantum States. *Phys. Rev. X* **2020**, *10*, 031064, doi:10.1103/PhysRevX.10.031064.
47. Gokhale, P.; Angiuli, O.; Ding, Y.; Gui, K.; Tomesh, T.; Suchara, M.; Martonosi, M.; Chong, F.T. $O(N^3)$ Measurement Cost for Variational Quantum Eigensolver on Molecular Hamiltonians. *IEEE Trans. Quantum Eng.* **2020**, *1*, 1–24, doi:10.1109/TQE.2020.3035814.
48. Ralli, A.; Love, P.; Tranter, A.; Coveney, P. Implementation of Measurement Reduction for the Variational Quantum Eigensolver. *arXiv* **2020**, arXiv:2012.02765.
49. Jordan, P.; Wigner, E. Über das Paulische Äquivalenzverbot. *Z. Phys.* **1928**, *47*, 631–651, doi:10.1007/BF01331938.
50. Aspuru-Guzik, A.; Dutoi, A.D.; Love, P.J.; Head-Gordon, M. Simulated quantum computation of molecular energies. *Science* **2005**, *309*, 1704–1707.
51. Somma, R.; Ortiz, G.; Gubernatis, J.E.; Knill, E.; Laflamme, R. Simulating physical phenomena by quantum networks. *Phys. Rev. A* **2002**, *65*, 042323.
52. Bravyi, S.B.; Kitaev, A.Y. Fermionic quantum computation. *Ann. Phys.* **2002**, *298*, 210–226.
53. Tranter, A.; Sofia, S.; Seeley, J.; Kaicher, M.; McClean, J.; Babbush, R.; Coveney, P.V.; Mintert, F.; Wilhelm, F.; Love, P.J. The Bravyi–Kitaev transformation: Properties and applications. *Int. J. Quantum. Chem.* **2015**, *115*, 1431–1441, doi:10.1002/qua.24969.
54. Kirby, W.M.; Love, P.J. Variational quantum eigensolvers for sparse Hamiltonians. *arXiv* **2020**, arXiv:2012.07171.
55. Abraham, H.; Akhalwaya, I.Y.; Aleksandrowicz, G.; Alexander, T.; Alexandrowics, G.; Arbel, E.; Asfaw, A.; Azaustre, C.; Barkoutsos, P.; Barron, G.; et al. Qiskit: An Open-source Framework for Quantum Computing. 2019. Available online: <https://zenodo.org/record/2562111#.YJufRahKhPZ> (accessed on 11 May 2021)
56. Kay, A. Quantikz. 2019. Available online: <https://royalholloway.figshare.com/articles/dataset/Quantikz/7000520/4> (accessed on 11 May 2021).
57. Hunter, J.D. Matplotlib: A 2D graphics environment. *Comput. Sci. Eng.* **2007**, *9*, 90–95.